JACS
JOURNAL OF THE AMERICAN CHEMICAL SOCIETY
Article
pubs.acs.org/JACS

Hole Removal Rate Limits Photodriven H_2 Generation Efficiency in CdS-Pt and CdSe/CdS-Pt Semiconductor Nanorod–Metal Tip Heterostructures

Kaifeng Wu, Zheyuan Chen, Hongjin Lv, Haiming Zhu, Craig L Hill, and Tianquan Lian*

Department of Chemistry, Emory University, Atlanta, Georgia 30322, United States

Supporting Information

ABSTRACT: Semiconductor–metal nanoheterostructures, such as CdSe/CdS dot-in-rod nanorods with a Pt tip at one end (or CdSe/CdS-Pt), are promising materials for solar-to-fuel conversion because they allow rational integration of a light absorber, hole acceptor, and electron acceptor or catalyst in an all-inorganic triadic heterostructure as well as systematic control of relative energetics and spatial arrangement of the functional components. To provide design principles of such triadic nanorods, we examined the photocatalytic H_2 generation quantum efficiency and the rates of elementary charge separation and recombination steps of CdSe/CdS-Pt and CdS-Pt nanorods. We showed that the steady-state H_2 generation quantum efficiencies (QEs) depended sensitively on the electron donors and the nanorods. Using ultrafast transient absorption spectroscopy, we determined that the electron transfer efficiencies to the Pt tip were near unity for both CdS and CdSe/CdS nanorods. Hole transfer rates to the electron donor, measured by time-resolved fluorescence decay, were positively correlated with the steady-state H_2 generation QEs. These results suggest that hole transfer is a key efficiency-limiting step. These insights provide possible ways for optimizing the hole transfer step to achieve efficient solar-to-fuel conversion in semiconductor–metal nanostructures.

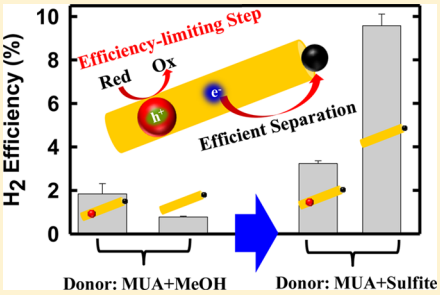

INTRODUCTION

Efficient artificial photosynthesis requires optimal integration of multiple functional components, including light absorbers, electron and hole acceptors, and catalysts.[1,2] It has been well demonstrated that in donor–light absorber–acceptor molecular triads, the spatial separation of electron donors and acceptors can lengthen the lifetime of charge-separated states and facilitate their coupling with catalysts for efficient selective light-driven oxidation or reduction reactions.[3−5] Recent advances in colloidal nanostructure synthesis have led to the development of triadic nanoheterostructures, in which multiple functional components are integrated in single all-inorganic structures and their spatial and energetics arrangements can be systematically optimized.[6−12] Compared to molecular systems, these all-inorganic nanostructures have superior long-term stability that is hard to achieve with molecular systems[13] and the energetics of the components can be readily tuned by their sizes through the quantum confinement effect.[14] For these reasons, a series of semiconductor–metal nanoheterostructures, especially platinum- or gold nanoparticle-decorated semiconductor nanorods (NRs) and nanowires have been successfully synthesized and investigated for photocatalysis applications.[11,12,15−22] Among them, CdSe/CdS dot-in-rod (DIR) nanorods with a platinum nanoparticle at one end (CdSe/CdS-Pt) serve as an ideal model system for examining the design principle of these triadic photocatalytic nanoheterostructures.[11] According to the relative energetics of CdSe, CdS, and Pt, photoexcitation in these triads can, in principle, lead to a long-lived charge separated-state with the electron at the Pt tip and the hole confined in the CdSe core that is tens of nanometers away. Indeed, in the presence of electron donors, these structures have been shown to carry out photoreduction of protons to form hydrogen molecules with a conversion quantum efficiency (QE) of as high as 20%.[11] Interestingly, the conversion QE appears to depend on the CdSe seed size and CdS rod length, suggesting the possibility of further optimization. Despite these reported promising performances, it is unclear what factors limit the overall QE of photoreduction and how QE depends on the chemical nature and dimension of the components.[23−25]

The photogeneration of H_2 in triadic nanoheterostructures such as CdSe/CdS DIR-Pt involves a series of desirable forward charge transfer and efficiency-reducing recombination processes, as shown in Figure 1c. Because of the quasi-type II band alignment between the CdSe seed and CdS rod, it is often thought that in the excited CdSe/CdS NRs, the valence band (VB) hole should localize to the CdSe seed (with a time constant of τ_{HL}) while the conduction band (CB) electron can delocalize between the CdS rod and CdSe seed, forming the lowest-energy exciton state in the heterostructure (labeled as X3 in Figure 1a).[26−29] However, the carrier relaxation dynamics and final locations of carriers in CdSe/CdS NRs are recently found to be excitation-energy dependent.[30,31] As shown in Figure 1a, our recent study reveals that after the rod excitation, in addition to X3, there exist two other distinct, long-lived

Received: March 9, 2014
Published: May 5, 2014

   dx.doi.org/10.1021/ja5023893 | J. Am. Chem. Soc. 2014, 136, 7708–7716

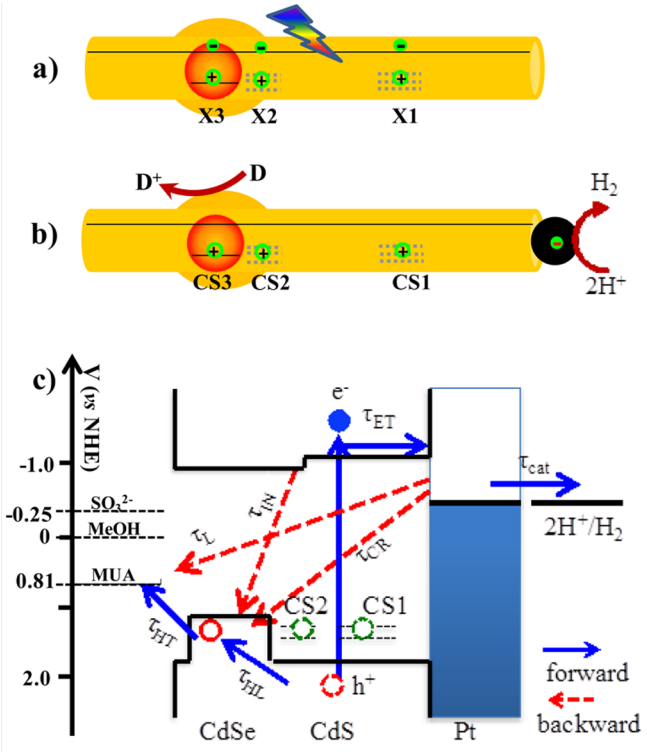

Figure 1. Photogeneration of H_2 using CdSe/CdS-Pt NRs. Schematic illustration of (a) three distinct exciton states (X1, X2, X3) in CdSe/CdS NRs and (b) three charge-separated states (CS1, CS2, CS3) in CdSe/CdS-Pt triadic nanoheterostructures with the hole localized in the CdS rod (X1 and CS1), CdS bulb region surrounding the seed (X2, CS2), and CdSe seed (X3, CS3). Also shown in (b) is the photocatalytic generation of H_2 from protons in the presence of electron donors D. (c) Simplified schematic energy levels and charge separation and recombination processes relevant to photocatalytic H_2 generation. The figure corresponds to the initial formation of CS3. The hole locations for CS1 and CS2 are also labeled (dashed green circles) for comparison. See the main text for details. All band edge positions and redox potentials correspond to aqueous solution at PH = 7, the condition for the photocatalytic experiments.

exciton states in CdSe/CdS NRs with the hole localized in the CdS rod (X1) and CdS bulb region surrounding the seed (X2).[30] As a result, further transfer of the electron to the Pt tip (with a time constant of τ_{ET}) should form three different charge-separated states with holes localized in the CdS rod (CS1), CdS bulb region (CS2), and CdSe core (CS3), as shown in Figure 1b. This is likely a common feature in CdSe/CdS-Pt nanorods, although the branching ratio for forming X1, X2, and X3 excitons, which is dependent on trap state density and morphology of the CdS rod, can vary among samples. For clarity, we have only depicted the relevant processes for CS3 in Figure 1c. Hole removal by electron donor D (with a time constant of τ_{HT}) enables the accumulation of electrons in the Pt tip to carry out reduction of two protons to form H_2 (with a time constant of τ_{CAT}). These forward processes compete with the recombination of electrons and holes within the NR (with an intrinsic lifetime of τ_{IN}), the loss of electrons in the Pt by charge recombination with the holes in the CdSe (with a time constant of τ_{CR}), and with the oxidized donor, D^+ (with a time constant of τ_L) and via other pathways. Thus, rational improvement of the photodriven hydrogen-generation efficiency in these materials requires a detailed understanding of these competing processes.

In this contribution, we examined the factors that limit the photocatalytic H_2 generation QE of CdSe/CdS-Pt and CdS-Pt NRs. The latter was included as a comparison to investigate the effect of quasi-type II band alignment in CdSe/CdS-Pt. We observed that the steady-state H_2 generation QE using these nanorods depended on the nature of the electron donor. With methanol as an electron donor, higher QE was observed for CdSe/CdS-Pt than for CdS-Pt. Using sulfite as an electron donor, the QEs were improved for both, but the QE for CdS-Pt became higher than that for CdSe/CdS-Pt. To investigate the mechanism of the observed electron donor dependent QE, we used transient absorption spectroscopy and time-resolved fluorescence decay to measure the charge separation, recombination, and hole removal rates in these systems. In all cases, the initial charge separation efficiency (electron transfer from NRs to Pt) was nearly 100% in these materials. The hole transfer rates were dependent on the nature of the electron donor and the NR, and correlated with the steady-state H_2 generation QEs. Thus, these results suggest that hole removal is the main efficiency-limiting factor in these systems. We discuss how these insights provide possible approaches for improving the photocatalytic H_2 generation properties of these nanoheterostructures.

RESULTS AND DISCUSSION

Absorption and Emission Properties of CdSe/CdS-Pt.

CdSe/CdS dot-in-rod NRs were prepared by a seeded-growth procedure.[32,33] Detailed characterization of the morphology, optical property, and exciton dynamics of these NRs has been published previously.[30] These CdSe/CdS NRs have an average length of 16.5 (±1.0) nm and a diameter of 3.5 (±0.3) nm, as well as a bulb region surrounding the CdSe seed with slightly larger diameter than the rest of the rod. The static absorption and emission spectra of CdSe/CdS NRs are displayed in Figure 2. The lowest absorption peak at ~540 nm (B3) can be

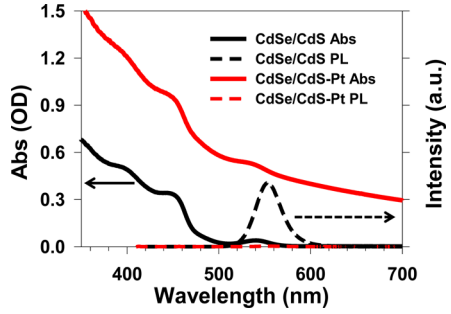

Figure 2. Static absorption (solid lines) and photoluminescence (PL, dashed lines) spectra of CdSe/CdS NRs (black lines) and CdSe/CdS-Pt NRs (red lines).

assigned to the X3 exciton transition (from the top of valence band in CdSe core to the lowest energy conduction band level), the pronounced peaks at ~450 nm (B1) and 400 nm can be attributed to the 1D excitonic transitions of the CdS rod region, and a small shoulder at 470 nm (B2) can be attributed to the transition from the VB top to the CB bottom of CdS in the bulb region surrounding the CdSe seed.[23,30] It is shown that the B2 and B3 transitions share the same CB electron level, reflecting the quasi-type II band alignment in this heterostructure. The photoluminescence (PL) spectrum of CdSe/CdS NRs measured with 400 nm excitation (Figure 2) was dominated by the emission of the X3 exciton state.

dx.doi.org/10.1021/ja5023893 | J. Am. Chem. Soc. 2014, 136, 7708−7716

Platinum deposition on the CdSe/CdS NRs was done by thermal reduction of Pt(II) acetylacetonate.[6] According to TEM images, the as-prepared CdSe/CdS-Pt heterostructures showed well-defined morphology, containing ~2%, 93%, and 5% NRs with 0, 1, and 2 Pt tips, respectively (Figure S1a and b in the Supporting Information [SI]). The absorption spectrum of CdSe/CdS-Pt (Figure 2) can be well modeled by a linear combination of CdSe/CdS and Pt contributions(Figure S2 in the SI). The latter is a broad featureless absorption tail extending to the near IR.[34] The PL of CdSe/CdS was completely quenched after the attachment of the Pt tips. We have also prepared CdS and CdS-Pt NR samples with similar dimensions (average rod length of 18.1 ± 1.8 nm and rod diameter of 3.5 ± 0.3 nm) according to previously published procedures.[6,33] Their static absorption spectra and TEM images are shown in Figure S7 in the SI.

Effect of Electron Donors on H_2 Generation Efficiency. We first compare the photocatalytic H_2 generation efficiencies of CdS-Pt and CdSe/CdS-Pt heterostructures. The as-prepared NR samples were capped by phosphonate ligands and dispersed in chloroform solutions. They were transferred to aqueous solutions by replacing the phosphonate ligands with 11-mercaptoundecanoic acid (MUA) according to ligand exchange procedures.[11,12] The steady-state H_2 generation measurements were carried out in reaction solutions of MUA-capped CdS-Pt or CdSe/CdS-Pt NRs in 1:10 volume ratio of methanol/water (methanol/MUA as electron donor) or in 0.1 M sodium sulfite water solution (sulfite/MUA as electron donor). As shown in Figure 1c, although the redox potential becomes more positive from sodium sulfite (−0.25 V vs NHE[36]) to methanol (~0 V vs NHE[35]) to MUA (~0.81 V vs NHE[36]), hole transfers from the CdSe and CdS valence bands to these molecules are energetically allowed. The optical densities of all the samples were adjusted to ~1.5 at 455 nm to ensure the same photon absorption rates in all solutions. The samples were illuminated by 455 nm LED light (15 mW), and H_2 was detected by gas chromatograph (see SI for further details). We first repeated previously reported experiments in which methanol was used as a sacrificial donor.[11] Figure 3a shows the H_2 evolution kinetics measured in the first 40 min of light illumination. The induction period, in the first 10 min, can be attributed to the solubility of H_2 in the aqueous solution[37] or remaining O_2 in the solution (due to imperfect purging of the system with argon).[38] After this period, the amounts of H_2 increase linearly with time, the slope of which indicates H_2 generation rate. From the ratio of H_2 generation and photon absorption rates, the photodriven H_2 generation QE can be calculated. After correcting for light absorption and scattering loss due to the cuvette and Pt particles, the internal QE is determined, as shown in Figure 3b. Using methanol as electron donor, the H_2 generation QEs of CdS-Pt and CdSe/CdS-Pt are 0.78 ± 0.03% and 1.8 ± 0.4%, respectively. These values are in good agreement with previous reports for NRs of similar lengths.[11]

Previous comparisons of photoreduction between CdSe/CdS-Pt and CdS-Pt[11] and between CdSe/CdS and CdS[39] have also reported higher efficiencies in CdSe/CdS NRs. The better performances in CdSe/CdS NRs have often been attributed to the quasi-type II band alignment between CdSe and CdS, which promotes internal electron−hole separation between the CdSe and CdS domains. If this was indeed the efficiency-limiting factor for these heterostructures, CdSe/CdS-Pt should have better performance than CdS-Pt under the same conditions regardless of the electron donors used. To test this hypothesis, we performed the same comparison of photocatalytic H_2 generation efficiencies of CdS-Pt and CdSe/CdS-Pt NRs using sodium sulfite/MUA as the electron donors. Their H_2 generation kinetics traces and the calculated internal QEs are shown in a and b of Figure 3, respectively. Compared to values measured with methanol/MUA as electron donors, the internal QEs for both samples are considerably higher and, more surprisingly, the QE of CdS-Pt (9.6 ± 0.5%) becomes 3 times higher than that of CdSe/CdS-Pt (3.2 ± 0.1%). This result indicates that H_2 generation efficiencies of CdS-Pt and CdSe/CdS-Pt depend strongly and in different ways on the electron donors. We note that the observed electron donor dependence in CdS-Pt NRs is consistent with a previous report by Berr et al.[40]

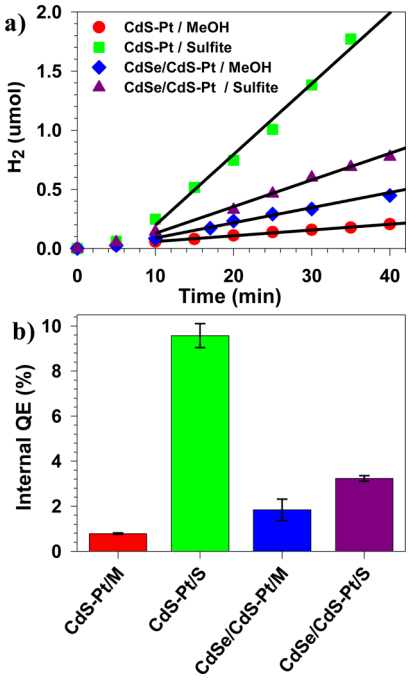

Figure 3. Steady-state H_2 photogeneration using MUA-capped CdSe/CdS-Pt and CdS-Pt NRs. (a) H_2 evolution kinetics traces for CdS-Pt with methanol (red circles) and sulfite (green squares), and CdSe/CdS-Pt with methanol (blue diamonds) and sulfite (purple triangles) as electron donors. The black solid lines are linear fits to the traces from 10 to 40 min, from which the H_2 generation rates were determined. (b) Calculated H_2 generation internal QEs for CdS-Pt and CdSe/CdS-Pt with methanol or sulfite electron donors.

Charge Separation and Recombination in Phosphonate-Capped CdSe/CdS-Pt and CdS-Pt. To unveil the mechanism for the observed nanorod and electron donor-dependent steady-state H_2 generation efficiencies, we carried out transient absorption and time-resolved fluorescence decay measurements of CdSe/CdS-Pt and CdS-Pt NRs to determine the rates of various competing processes shown in Figure 1c. We first measured the rates of electron transfer (τ_{ET}) from these nanorods to the Pt tip and the subsequent charge recombination (τ_{CR}) processes in the absence of a hole acceptor. Because thiol is a hole acceptor, for this experiment, we used NRs capped by phosphonate and dispersed in chloroform solution. By comparing with intrinsic exciton lifetime measured in CdSe/CdS and CdS nanorods without Pt tips, we determined the QE for the initial charge separation (i.e., electron transfer to Pt) process.

dx.doi.org/10.1021/ja5023893 | J. Am. Chem. Soc. 2014, 136, 7708−7716

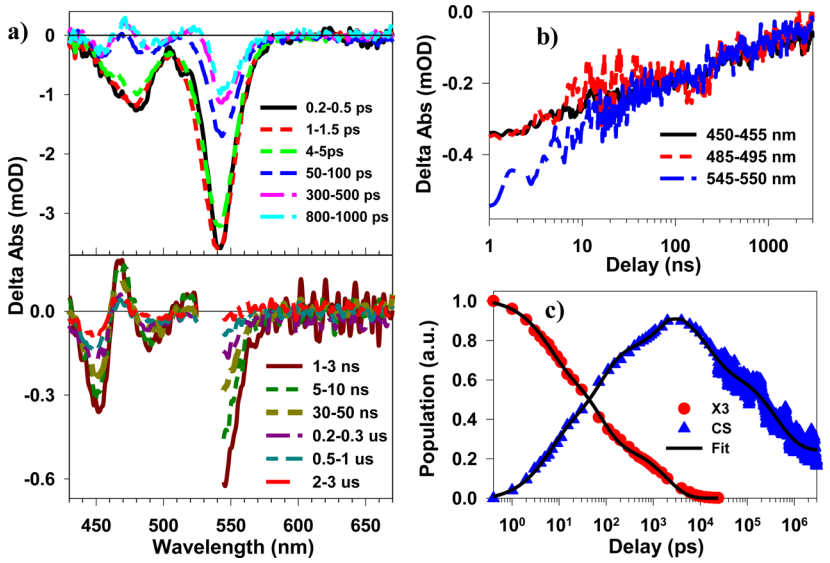

Figure 4. Transient absorption spectra and kinetics of CdSe/CdS-Pt measured at 540 nm excitation. (a) Transient absorption spectra of CdSe/CdS-Pt at indicated time delays: 0.2 to 1000 ps (upper panel) and 1 to 3000 ns (lower panel). (b) Kinetics probed at indicated wavelength ranges from 1 to 3000 ns. (c) Time-dependent populations for X3 (red circles) and charge-separated states (CS, blue triangles) from 0.4 ps to 3000 ns extracted from fitting the TA spectra (see main text) and their fits to multiexponential functions (black solid lines).

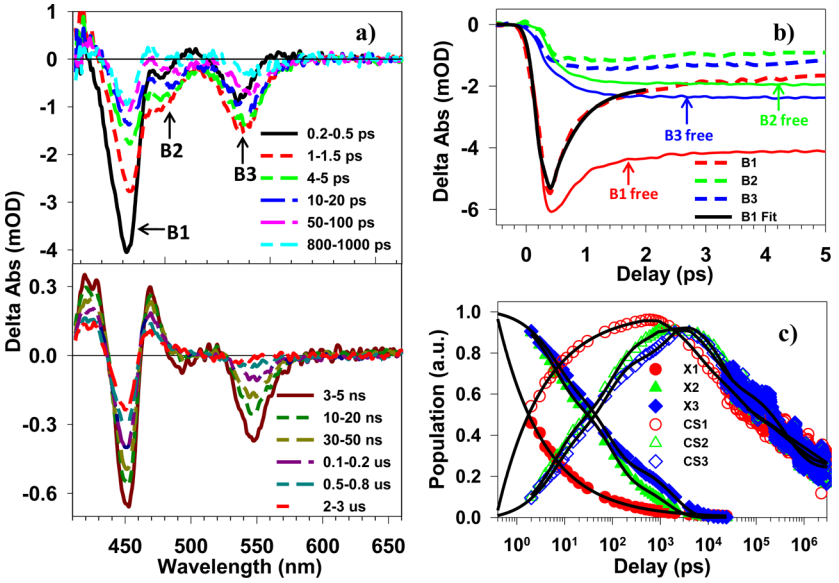

Figure 5. Transient absorption spectra and kinetics of CdSe/CdS-Pt measured with 400 nm excitation. (a) TA spectra of CdSe/CdS-Pt at indicated delay times: (upper panel) 0.2 to 1000 ps, showing charge-separation process, and (lower panel) 3 to 3000 ns, showing mostly the charge-recombination process. (b) Kinetics of B1 (~450 nm, red lines), B2 (~480 nm, green line), and B3 (~540 nm, blue line) of CdSe/CdS-Pt (dashed lines) and CdSe/CdS (solid lines) within 5 ps. The black solid line is a fit to B1 kinetics within 2 ps. (c) Time-dependent populations for X1 (red filled circles), X2 (green filled triangles), X3 (blue filled diamonds) excitons and their charge-separated states CS1(red open circles), CS2 (green open triangles), and CS3 (blue open diamonds) from 0.4 ps to 3000 ns. The black solid lines are multiexponential fits to these kinetics.

X3 Exciton Charge Separation/Recombination in CdSe/CdS-Pt. As illustrated in Figure 1a, optical excitation of CdSe/CdS at 455 nm creates an electron−hole pair in the CdS rod region that can decay by three pathways to form X1, X2, and X3 excitons.[30] To simplify the data analysis, we first measured TA spectra with 540 nm pump pulse, which selectively excited the lowest-energy exciton band and generated only the X3 exciton state in the NR.[30] As shown in Figure S3a in the SI, X3 in free CdSe/CdS NRs is long-lived with a half-life of ~8.3 ns.[30] Figure 4a shows the TA spectra of CdSe/CdS-Pt at indicated time delays after 540 nm excitation. The TA spectrum at early delay time (<1 ps) shows two pronounced bleach of B3 (540 nm) and B2 (475 nm) transitions, similar to free CdSe/CdS NRs. These features have been attributed to CB electron state-filling-induced bleaches, which provide a convenient probe of the lifetime of the X3 excitons.[30,41] The presence of X3 exciton also leads to the bleach of B2 transition, indicating that the lowest-energy CB electron level extends into the CdS bulb region, consistent with the quasi-type II band alignment in this heterostructure. Compared to free CdSe/CdS NRs, these bleach features recover with a much faster rate, indicating shorter-lived CB electrons. Accompanying the decay of X3 signals are derivative-like features formed in the range of 430−500 nm. Similar features are commonly observed in the TA

dx.doi.org/10.1021/ja5023893 | J. Am. Chem. Soc. 2014, 136, 7708−7716

spectra of quantum dot−acceptor complexes and are attributed to charge separation-induced Stark effect signals (CS).[30,42,43] Therefore, both the fast bleach recovery and CS spectral signatures confirm photoinduced electron transfer from the CdSe/CdS NR to the Pt tip. The lower panel of Figure 4a shows that the CS features decay from 1 to 3000 ns due to the recombination of the electron in the Pt tip with the VB hole in the CdSe core.

The rates of charge separation and recombination processes were measured by following the decay kinetics of X3 exciton bleach and CS signals, respectively. Due to spectral and temporal overlaps of these two signals, we fit the TA spectra as a linear combination of X3 and CS signals to obtain the time-dependent X3 and CS coefficients, which were used to construct the charge separation and recombination kinetics, respectively.[30] The TA spectrum of DIR-Pt at 1 ps was taken as the pure X3 spectrum, and the TA spectrum averaged from 30 to 50 ns the pure CS spectrum. This is justified by the fact that charge separation is completed at 30 ns, after which all the spectral features decay in the same way, as shown in Figure 4b. TA spectra from 0.4 ps to 30 ns were fitted, and the detailed procedures as well as the fitted spectra are shown in the SI (Figure S4). The time-dependent population coefficients for X3 and CS signals obtained from the fit are displayed in Figure 4c. Note that the coefficients for CS after 30 ns were directly taken from TA kinetics at 453 nm which were scaled and connected with the fitted coefficients. The X3 and CS kinetics were fitted with multiexponential functions, from which half-lives of 43.5 ± 4.7 ps and 211 ± 38 ns for charge separation and recombination, respectively, were obtained. The fitting procedures and parameters are provided in the SI (Table S1).

Charge Separation/Recombination in CdSe/CdS-Pt Following CdS Rod Excitation. For CdSe/CdS NRs, absorption at wavelengths shorter than 460 nm is dominated by transitions within the CdS rod due to its large volume and absorption cross section.[27] To mimic the initial absorption conditions created by 455 nm excitation used in the steady-state H_2 generation experiment, we measured transient absorption spectra of phosphonate-capped CdSe/CdS (Figure S3b in the SI) and CdSe/CdS-Pt NRs at 400 nm excitation. We have previously shown that the e−h pairs generated with 400 nm excitation of CdS rods relax into three spatially separated excitons: X1, X2, and X3, as shown in Figure 1a, with formation probabilities and half-lives of (~46%, 22.5 ns), (7%, 32.1 ns), and (47%, 8.3 ns), respectively.[30] The formation of X1, X2, and X3 is driven by hole localization from the CdS rod valence band to trap states at the CdS rod (with a time constant of τ_{HL1} = 0.48 ps), the CdS bulb (τ_{HL2} = 0.42 ps), and CdSe seed (τ_{HL3} = 0.42 ps), respectively.

The TA spectra of CdSe/CdS-Pt at indicated delay times following 400 nm excitation are shown in Figure 5a. The bleaches at the B1, B2, and B3 transitions recovered quickly with concomitant formation of derivative-like charge-separated state (CS) signals. The initial signal amplitudes of B2 and B3 were only 67% of those in free DIRs (Figure 5b), suggesting ultrafast electron transfer to Pt prior to the formation of X2 and X3. From the signal amplitudes of B2 and B3 and the kinetics of B1, the time constant of fast electron transfer process from these free excitons was determined to be τ_{ET} = 0.47 ps (see SI for details).

After 2 ps, all the exciton localization processes were completed, and the TA spectra could be fitted to a linear combination of exciton state filling and CS signals for X1, X2, and X3 excitons. Detailed description of the fitting procedure is given in the SI. Briefly, the spectra of X1, X2, and X3 have been identified previously (Figure S6a in the SI). The charge separation and recombination rates as well as charge-separated state spectra (CS3) of X3 excitons have been independently determined in the measurement with 540 nm excitation (Figure 4). Because exciton X2 and X3 share the same conduction band electron level (due to quasi-type II band alignment) and have holes localized in the bulb region, we assume that the dissociation of these excitons generates charge-separated states, CS2 and CS3, respectively, with similar Stark effect TA spectra and lifetimes. Subtracting their contribution from the TA spectrum at 30 ns (measured with 400 nm excitation), consisting of the CS states (CS1+CS2+CS3) only, yields CS1 TA spectrum. The time-dependent population coefficients for X1, X2, X3 and CS1, CS2, and CS3 signals obtained from fitting the TA spectra are displayed in Figure 5c. These kinetics were fitted to multiexponential functions, and the fitting parameters are listed in Table S2 in the SI. From the fit, we obtained half-lives of 1.75 ± 0.22 ps, 30.1 ± 3.5, and 43.5 ± 4.7 ps for charge separation and 102 ± 29 ns, 211 ± 38 ns, and 211 ± 38 ns for charge recombination for X1, X2, and X3 excitons, respectively. Further details of the fitting procedure are discussed in the SI.

Comparing Charge Separation/Recombination in CdSe/CdS-Pt and CdS-Pt. As a comparison, we have also measured TA spectra of CdS-Pt with 400 nm excitation, as shown in Figure S8 in the SI. The assignment of spectral signatures in CdS-Pt nanorods and the extraction of charge separation and recombination rates from the TA spectra have been reported previously and are briefly described in the SI.[23] The half-lives for charge separation and recombination in CdS-Pt were determined to be 2.15 ± 0.35 ps and 149 ± 52 ns, respectively.

Due to significant spectral overlap between CdSe/CdS emission and Pt absorption (Figure 2), the possibility of energy transfer should be considered.[44,45] We have estimated the energy transfer rate from the X3 exciton state, the main emissive state in CdSe/CdS NRs, to the Pt tip based on the Forster resonant energy transfer (FRET) model.[46] As shown in the SI, the estimated upper limit of energy transfer rate is ~1/38.7 ns^{-1}, which is too slow to compete with electron transfer from X3 to Pt. In addition, we have previously shown that energy transfer from CdS NR to Pt tip cannot compete with electron transfer either, due to an ultrafast hole-trapping process.[23,47]

Listed in Table 1 are the charge separation and recombination rates for CdSe/CdS-Pt and CdS-Pt measured

Table 1. Comparison of Charge Separation (τ_{CS}), Charge Recombination (τ_{CR}), and Intrinsic Half Lifetimes (τ_{IN}) in CdSe/CdS-Pt and CdS-Pt

	CdSe/CdS -Pt			CdS -Pt
	X1	X2	X3	
τ_{CS} (ps)	1.75±0.22	30.1±3.5	43.5±4.7	2.15±0.35
τ_{CR} (ns)	102±29 ns	211±38 ns	211±38 ns	149±52 ns
τ_{IN} (ns)	22.5±1.7*	32.1±2.2*	8.34±0.31*	24.7±0.9
Φ (%)	99.99	99.91	99.47	99.99
Φ_{eff}(%)	99.82			99.99

*Taken from ref 30.

dx.doi.org/10.1021/ja5023893 | J. Am. Chem. Soc. 2014, 136, 7708−7716

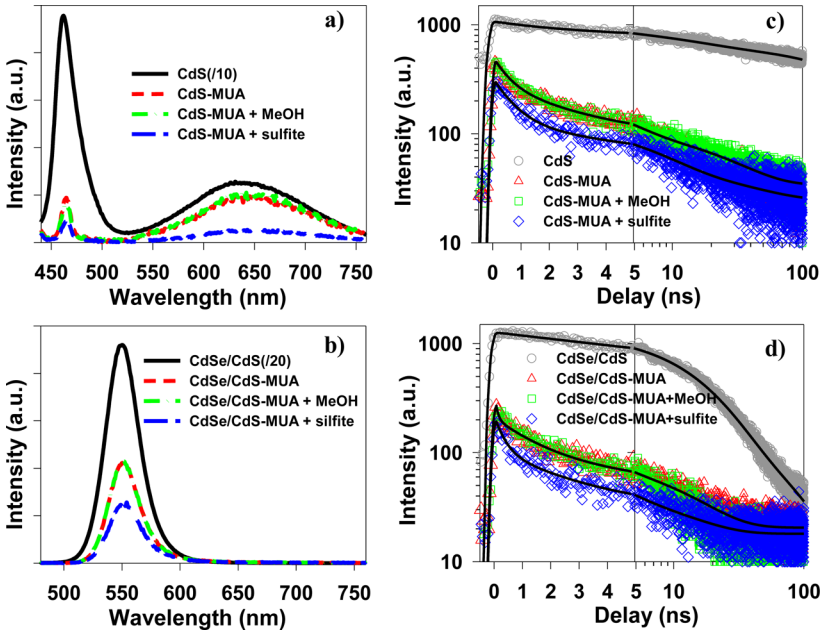

Figure 6. Static PL spectra (a,b) and PL decay kinetics (c, d) of CdS (a,c) and CdSe/CdS (b,d) NRs. Four samples are compared in each panel: phosphonate-capped NRs in chloroform (black solid line or circles) and MUA-capped NRs in in water (red dashed line, triangles), in 1:10 volume ratio of methanol/water (green dashed−dotted line or squares), and in 0.1 M sodium sulfite water solution (blue dashed line or diamonds). All samples were excited at 400 nm. The PL kinetics were measured between 532 and 675 nm. The black solid lines in (c) and (d) are multiexponential fits with parameters listed in Table S4 in the SI.

at 400 nm excitations, along with the intrinsic exciton lifetimes in free CdSe/CdS and CdS NRs. We define the charge separation yield (Φ) as $\Phi = ((1/\tau_{CS}) - (1/\tau_{IN}))/(1/\tau_{CS}) = (\tau_{IN} - \tau_{CS})/\tau_{IN}$, where τ_{IN} and τ_{CS} are the conduction band electron half-lives in NRs without and with Pt tips, respectively. τ_{IN} depends on the "intrinsic" radiative and nonradiative decay processes within the semiconductor domain (in the absence of the Pt tip). We have assumed that the growth of the Pt tip adds an electron transfer pathway ($1/\tau_{ET}$) and does not affect the rate of the intrinsic decay processes ($1/\tau_{CS} = 1/\tau_{ET} + 1/\tau_{IN}$). For CdSe/CdS NRs, three types of excitons have their individual charge separation yields. Therefore, the population-weighted charge-separation yield is taken as the effective yield: $\Phi_{eff} = \sum_{i=1}^{3} a_i\Phi_i$, where a_i and Φ_i are the population percentage and charge-separation yield for exciton Xi (i = 1,2,3) in CdSe/CdS-Pt NRs. The calculated Φ values for both CdS-Pt and CdSe/CdS-Pt (listed in Table 1) are nearly 100%, indicating that all excitons in the semiconductor domain dissociate by electron transfer to the Pt tip. Therefore, the charge separation efficiencies in DIR-Pt and NR-Pt are not the factor that limits the photocatalytic efficiency.

Although efficient charge separation and long-lived charge-separated states are achieved in both CdSe/CdS-Pt and CdS-Pt NRs, there are interesting differences in their mechanisms. In CdS-Pt NRs, rapid trapping of holes on CdS NR surface generates a charge-separated state with long lifetime. In CdSe/CdS-Pt NRs, there exist three excitons. The charge-separated states resulting from X1 and X2 (53% of the total population) excitons are similar to those of CdS-Pt nanorods. It should be noted that the X2 exciton is not explicitly considered in our analysis of the TA spectra of CdS-Pt NRs because its contribution, dependent on sample growth conditions, is too small to be accurately determined. The X3 exciton leads to long-lived charge-separated state by localizing the hole at the CdSe seed far away from the Pt tip. In comparison, instead of the poorly understood surface traps on CdS rod, localization of hole on CdSe seed may provide a better path toward rational control of the distance (and lifetime) of charge separation in CdSe/CdS-Pt and other dot-in-rod NRs.

Hole Filling of CdSe/CdS and CdS NRs by Electron Donor. As shown in Figure 1b, in addition to efficient charge separation, charge accumulation and turnover on the Pt catalyst requires fast hole removal to suppress the charge recombination processes.[12,39,40] As shown above, TA signals are dominated by contributions of electron-state filling-induced exciton bleach and are less sensitive to the dynamics of hole transfer. Hole transfer rates to electron donors can be measured by time-resolved photoluminescence (PL) decay of CdS and CdSe/CdS NRs (without Pt tip) in the presence of electron donors. These experiments were performed in aqueous solutions using MUA-capped NRs under conditions used for the steady-state photocatalytic H_2 generation measurements. In addition to methanol and sodium sulfite, the native ligand, MUA (~0.81 V vs NHE[36]), is an efficient donor itself, and the hole filling rate by MUA can be extracted by comparing the PL decay rates of MUA-capped NRs in aqueous solution and phosphonate-capped NRs in organic solvents.[12,39,48] Parts a and b of Figure 6 show the static PL spectra of CdS and CdSe/CdS NRs, respectively, in the presence of different electron donors after 400 nm excitation. The PL intensities of CdS and CdSe/CdS NRs were quenched by 22- and 45-folds, respectively, upon exchanging the phosphonate by MUA ligands, indicating that MUA is an effective hole acceptor. Adding methanol into the aqueous solution of MUA-capped CdS and CdSe/CdS NRs had negligible effects on the PL intensities. In contrast, in the presence of 0.1 M of sodium sulfite, the PL of NRs and DIRs were further quenched to ~25% and ~63% of MUA-capped NRs, respectively.

To determine the hole transfer (HT) rates, we also measured the PL decay kinetics for these samples between 532 and 675

dx.doi.org/10.1021/ja5023893 | J. Am. Chem. Soc. 2014, 136, 7708−7716

Table 2. Apparent Hole Transfer Times and H_2 Generation Quantum Efficiency (QE)

	CdS-Pt+MeOH		CdS-Pt+sulfite		CdSe/CdS-Pt+MeOH		CdSe/CdS-Pt+sulfite	
Apparent HT (ns)	MUA	MeOH	MUA	sulfite	MUA	MeOH	MUA	sulfite
	0.218 ±0.003	>>100	0.218± 0.003	0.0607 ±0.018	0.0441 ±0.008	>>100	0.0441 ±0.008	0.154 ±0.022
QE (H_2)	0.78±0.03%		9.6±0.5%		1.8±0.4%		3.2±0.1%	

nm after 400 nm excitation. For CdS NRs, PL in this spectral region is dominated by the broad trap-mediated emission band (Figure 6a), which is shown to be the main recombination channel because of the fast trapping of photogenerated holes.[23] For CdSe/CdS NRs, it probes the emission from the X3 exciton, which accounts for 47% of the excited NRs. The remaining 53% of excitons are localized on the CdS rod, whose emission quantum yield (~0.2%) is too small to be accurately measured in the presence of the much stronger X3 exciton emission (QE ≈ 48%). The PL intensities of NRs with and without electron donors were measured under the same conditions (excitation power and sample absorbance), such that both the absolute intensities and decay times can be compared. Compared to phosphonate-capped NRs (Figure 6c and d), the PL of MUA-capped NRs shows a smaller initial amplitude and faster decay. The former indicates a PL decay component that is faster than the instrument response (~240 ps). PL decay kinetics of MUA-capped NRs was not affected by the addition of methanol, but was affected by sulfite, consistent with the effect of these electron donors on the steady emission intensity (Figure 6a and b). To quantify the hole-transfer rates, these kinetics were fitted to multiexponential decay functions. From the fitting parameters, listed in Table S4 in the SI, we calculated the amplitude-weighted average PL decay rate for NRs ($k_{ave,NR}$), NRs with MUA ($k_{ave,NR-MUA}$) and NRs with MUA and sulfite ($k_{ave,NR-MUA+silfite}$). The hole transfer rates to MUA and sulfite were then calculated according to eqs 1 and 2.[49,50]

$$k_{HT,MUA} = k_{ave,NR-MUA} - k_{ave,NR} \quad (1)$$

$$k_{HT,sulfite} = k_{ave,NR-MUA+sulfite} - k_{ave,NR-MUA} \quad (2)$$

The calculated average hole transfer times ($\tau_{HT,i} = 1/k_{HT,i}$ are listed in Table 2. Hole transfer times from both CdS and CdSe/CdS NRs to methanol were too slow to be determined (≫100 ns). Hole transfer rate from CdSe/CdS to MUA was ~4.9 times faster than CdS, while hole transfer from CdS to sulfite was ~2.5 times faster than CdSe/CdS. We speculate that the differences in hole transfer rates can be qualitatively understood from the nature and location of the holes in CdS and CdSe/CdS NRs. The broad trap-mediated emission in CdS NRs is often attributed to a broad distribution of trapping states,[51] but a recent model suggests that it can also be caused by localized holes with strong coupling to phonons.[52,53] As shown in Figure 6a, the observed quenching of trap emission shows negligible wavelength dependence, which is consistent with the latter model. A strong coupling between holes and phonons requires a larger reorganization energy and driving force for fast hole transfer.[52−54] In CdSe/CdS NRs, the VB holes are localized in the CdSe seed, well separated from the surface by the CdS shell.[32,33] Therefore, in the case of weakly reductive MUA (~0.81 V vs NHE[36]), the rate for transferring the surface-trapped holes in CdS NRs is slower than the VB holes from the CdSe seed. In contrast, the more strongly reductive sulfite (−0.25 V vs NHE[36]) provides a larger driving force for removing the surface-trapped holes in CdS NRs.[36] In this case, the hole transfer rate becomes slower in CdSe/CdS due to its confinement within the CdSe core that is harder to access by the electron donor. Hole transfer rates likely depend also on the interaction of hole acceptors with surface-capping ligands and the accessibility of surface sites. It is unclear how the difference in these factors contributes to the observed trend of hole transfer rates. It should be noted a previous study has reported a positive correlation between H_2 generation efficiency in CdS-Pt NRs with the reducing power of the electron donor.[40] Our result suggests that this correlation may result from faster hole transfer rates from CdS-Pt NRs to donors with more negative reduction potential.[40]

The measured average hole transfer times and H_2 generation QEs for CdS and CdSe/CdS NRs are compared in Table 2, which shows a positive correlation between the hole transfer rate and H_2 generation QE. Specifically, (i) the H_2 generation QEs and hole transfer rates are higher with sulfite than methanol for both NRs, and (ii) the relative QE follows the trend of hole transfer rates when comparing CdS-Pt with CdSe/CdS-Pt NRs. Furthermore, a control experiment showed that methanol has negligible effects on the H_2 generation QEs of MUA-capped NR-Pt (Figure S9 in the SI), which is consistent with its negligible effects on the hole transfer rates (from both PL decay and static PL quenching of NRs). The positive correlation between hole transfer rate and H_2 generation QE and the observed unity quantum yield for the initial charge separation suggests that hole removal is an efficiency-limiting step in photocatalytic H_2 generation using these NR heterostructures. Indeed, previous studies of CdS naonparticles show that using a mixture of sulfite and sulfide (S^{2-}/SO_3^{2-}) as electron donors can lead to H_2 generation efficiencies higher than 50%.[55−58] This may be attributed to the higher reduction power of S^{2-} (−0.45 V vs NHE[59]), which should give rise to faster hole removal rates. We have avoided using sulfide in this study because it can lead to charging of nanocrystals and complicate the assignment of measured PL intensities and lifetimes.[60] It should be noted that sulfite appeared to have negligible effect on the absorption spectra of the QD, suggesting negligible degree of QD charging.[60]

The H_2 generation QE of CdS-Pt obtained with sulfite electron donor (9.6%) is comparable to the highest reported values for these colloidal heterostructrues.[18,36,39,61] However, the steady-state H_2 generation efficiency is still far from unity, despite the unity initial quantum yield of electron transfer to Pt. According to Tables 1 and 2, the removal rates of holes in CdSe core or on CdS surface traps by electron donors are considerably faster than the rates of their recombination with the electrons in Pt. This result may suggest that the holes that

dx.doi.org/10.1021/ja5023893 | J. Am. Chem. Soc. 2014, 136, 7708−7716

are transferred to MUA or to sulfite (i.e., the one-electron oxidized sulfite and MUA intermediate) can still recombine with electrons in Pt, reducing the H_2 generation efficiency.[38]

The findings of this study suggest possible pathways for designing more efficient solar-to-fuel conversion systems using semiconductor−metal nanostructures. The first approach is to use hole scavengers with faster hole transfer rates. While using more reductive donors such as S^{2-} and SO_3^{2-} can achieve the goal by providing large drive forces for hole transfer,[38,55−57,62] it reduces the net energy gain in (and hence the solar-to-fuel energy conversion efficiency of) the fuel-forming reaction. Another way to improve hole transfer rates is to utilize electron donors that can more readily access the NR surface. The morphology of the nanorod can be optimized to expose the hole-trapping domains to the electron donor. For example, a recent study showed that etching the lateral dimension of CdSe/CdS NRs could significantly increase the H_2 generation rate because it exposed the hole-containing CdSe core to the electron donors.[17] Alternatively, NR growth methods that can locate the CdSe seed (or other hole-containing seed) at one end of the rod structure should also improve the hole transfer rate.

CONCLUSION

In conclusion, we have observed electron donor- and nanorod structure-dependent photocatalytic H_2 generation performances of MUA-capped CdSe/CdS-Pt and CdS-Pt NRs. Compared to methanol, using sulfite as electron donor improves the H_2 generation QEs for both NRs. The relative performance of these two NRs depended on the nature of the electron donor: higher QE was observed for CdSe/CdS-Pt using MUA/methanol, while with MUA/sulfite higher QE was achieved in CdS-Pt. Using ultrafast transient absorption spectroscopy, we showed that electron transfer efficiencies to the Pt tip were near unity for both CdS and CdSe/CdS NRs. The transfer rates of holes localized at the CdS rod surface and CdSe seed were measured by time-resolved PL decay. We found a positive correlation of the observed hole transfer rates with the steady-state H_2 generation quantum yields, indicating that hole transfer was a key efficiency-limiting step. Our finding suggests that the H_2 generation quantum efficiency can be further improved by using faster hole acceptors or designing nanorod structures that facilitate hole transfer.

ASSOCIATED CONTENT

Supporting Information

Sample preparations, pump−probe transient absorption spectroscopy and time-resolved fluorescence lifetime setup, light-driven H_2 generation experiment, estimation of energy transfer rate between CdSe core in DIR and Pt tip, fitting details on charge separation and recombination kinetics in DIR-Pt and NR-Pt ,and hole transfer kinetics of NRs and DIRs with different sacrificial donors. This material is available free of charge via the Internet at http://pubs.acs.org.

AUTHOR INFORMATION

Corresponding Author

tlian@emory.edu

Notes

The authors declare no competing financial interest.

ACKNOWLEDGMENTS

We acknowledge the financial supports from the Office of Basic Energy Sciences of the U.S. Department of Energy (Grant No. DE-FG02-12ER16347).

REFERENCES

(1) Alstrum-Acevedo, J. H.; Brennaman, M. K.; Meyer, T. J. *Inorg. Chem.* **2005**, *44*, 6802.
(2) Nocera, D. G. *Acc. Chem. Res.* **2012**, *45*, 767.
(3) Gust, D.; Moore, T. A.; Moore, A. L. *Acc. Chem. Res.* **2000**, *34*, 40.
(4) Liddell, P. A.; Kuciauskas, D.; Sumida, J. P.; Nash, B.; Nguyen, D.; Moore, A. L.; Moore, T. A.; Gust, D. *J. Am. Chem. Soc.* **1997**, *119*, 1400.
(5) Wasielewski, M. R. *Chem. Rev.* **1992**, *92*, 435.
(6) Habas, S. E.; Yang, P.; Mokari, T. *J. Am. Chem. Soc.* **2008**, *130*, 3294.
(7) Dukovic, G.; Merkle, M. G.; Nelson, J. H.; Hughes, S. M.; Alivisatos, A. P. *Adv. Mater.* **2008**, *20*, 4306.
(8) Shi, W.; Zeng, H.; Sahoo, Y.; Ohulchanskyy, T. Y.; Ding, Y.; Wang, Z. L.; Swihart, M.; Prasad, P. N. *Nano Lett.* **2006**, *6*, 875.
(9) Mokari, T.; Rothenberg, E.; Popov, I.; Costi, R.; Banin, U. *Science* **2004**, *304*, 1787.
(10) Tang, M. L.; Grauer, D. C.; Lassalle-Kaiser, B.; Yachandra, V. K.; Amirav, L.; Long, J. R.; Yano, J.; Alivisatos, A. P. *Angew. Chem., Int. Ed.* **2011**, *50*, 10203.
(11) Amirav, L.; Alivisatos, A. P. *J. Phys. Chem. Lett.* **2010**, *1*, 1051.
(12) Acharya, K. P.; Khnayzer, R. S.; O'Connor, T.; Diederich, G.; Kirsanova, M.; Klinkova, A.; Roth, D.; Kinder, E.; Imboden, M.; Zamkov, M. *Nano Lett.* **2011**, *11*, 2919.
(13) Kamat, P. V. *J. Phys. Chem. C* **2008**, *112*, 18737.
(14) Brus, L. E. *J. Chem. Phys.* **1983**, *79*, 5566.
(15) Berr, M.; Vaneski, A.; Susha, A. S.; Rodriguez-Fernandez, J.; Doblinger, M.; Jackel, F.; Rogach, A. L.; Feldmann, J. *Appl. Phys. Lett.* **2010**, *97*, 093108.
(16) Berr, M. J.; Schweinberger, F. F.; Döblinger, M.; Sanwald, K. E.; Wolff, C.; Breimeier, J.; Crampton, A. S.; Ridge, C. J.; Tschurl, M.; Heiz, U.; Jäckel, F.; Feldmann, J. *Nano Lett.* **2012**, *12*, 5903.
(17) Khon, E.; Lambright, K.; Khnayzer, R. S.; Moroz, P.; Perera, D.; Butaeva, E.; Lambright, S.; Castellano, F. N.; Zamkov, M. *Nano Lett.* **2013**, *13*, 2016.
(18) Tongying, P.; Plashnitsa, V. V.; Petchsang, N.; Vietmeyer, F.; Ferraudi, G. J.; Krylova, G.; Kuno, M. *J. Phys. Chem. Lett.* **2012**, *3*, 3234.
(19) Bang, J. U.; Lee, S. J.; Jang, J. S.; Choi, W.; Song, H. *J. Phys. Chem. Lett.* **2012**, *3*, 3781.
(20) Elmalem, E.; Saunders, A. E.; Costi, R.; Salant, A.; Banin, U. *Adv. Mater.* **2008**, *20*, 4312.
(21) Ha, J. W.; Ruberu, T. P. A.; Han, R.; Dong, B.; Vela, J.; Fang, N. *J. Am. Chem. Soc.* **2014**, *136*, 1398.
(22) Tongying, P.; Vietmeyer, F.; Aleksiuk, D.; Ferraudi, G. J.; Krylova, G.; Kuno, M. *Nanoscale* **2014**, *6*, 4117.
(23) Wu, K.; Zhu, H.; Liu, Z.; Rodríguez-Córdoba, W.; Lian, T. *J. Am. Chem. Soc.* **2012**, *134*, 10337.
(24) O'Connor, T.; Panov, M. S.; Mereshchenko, A.; Tarnovsky, A. N.; Lorek, R.; Perera, D.; Diederich, G.; Lambright, S.; Moroz, P.; Zamkov, M. *ACS Nano* **2012**, *6*, 8156.
(25) Berr, M. J.; Vaneski, A.; Mauser, C.; Fischbach, S.; Susha, A. S.; Rogach, A. L.; Jäckel, F.; Feldmann, J. *Small* **2012**, *8*, 291.
(26) Lupo, M. G.; Della Sala, F.; Carbone, L.; Zavelani-Rossi, M.; Fiore, A.; Lüer, L.; Polli, D.; Cingolani, R.; Manna, L.; Lanzani, G. *Nano Lett.* **2008**, *8*, 4582.
(27) Borys, N. J.; Walter, M. J.; Huang, J.; Talapin, D. V.; Lupton, J. M. *Science* **2010**, *330*, 1371.
(28) Talapin, D. V.; Koeppe, R.; Götzinger, S.; Kornowski, A.; Lupton, J. M.; Rogach, A. L.; Benson, O.; Feldmann, J.; Weller, H. *Nano Lett.* **2003**, *3*, 1677.
(29) She, C.; Demortière, A.; Shevchenko, E. V.; Pelton, M. *J. Phys. Chem. Lett.* **2011**, *2*, 1469.

(30) Wu, K.; Rodríguez-Córdoba, W. E.; Liu, Z.; Zhu, H.; Lian, T. *ACS Nano* **2013**, *7*, 7173.
(31) She, C.; Bryant, G. W.; Demortière, A.; Shevchenko, E. V.; Pelton, M. *Phys. Rev. B* **2013**, *87*, 155427.
(32) Talapin, D. V.; Nelson, J. H.; Shevchenko, E. V.; Aloni, S.; Sadtler, B.; Alivisatos, A. P. *Nano Lett.* **2007**, *7*, 2951.
(33) Carbone, L.; Nobile, C.; De Giorgi, M.; Sala, F. D.; Morello, G.; Pompa, P.; Hytch, M.; Snoeck, E.; Fiore, A.; Franchini, I. R.; Nadasan, M.; Silvestre, A. F.; Chiodo, L.; Kudera, S.; Cingolani, R.; Krahne, R.; Manna, L. *Nano Lett.* **2007**, *7*, 2942.
(34) Johnson, R. C.; Li, J.; Hupp, J. T.; Schatz, G. C. *Chem. Phys. Lett.* **2002**, *356*, 534.
(35) Iwasita, T. *Electrochim. Acta* **2002**, *47*, 3663.
(36) Brown, K. A.; Wilker, M. B.; Boehm, M.; Dukovic, G.; King, P. W. *J. Am. Chem. Soc.* **2012**, *134*, 5627.
(37) Toshima, N.; Takahashi, T.; Hirai, H. *J. Macromol. Sci., Chem.* **1988**, *25*, 669.
(38) Buehler, N.; Meier, K.; Reber, J. F. *J. Phys. Chem.* **1984**, *88*, 3261.
(39) Zhu, H.; Song, N.; Lv, H.; Hill, C. L.; Lian, T. *J. Am. Chem. Soc.* **2012**, *134*, 11701.
(40) Berr, M. J.; Wagner, P.; Fischbach, S.; Vaneski, A.; Schneider, J.; Susha, A. S.; Rogach, A. L.; Jackel, F.; Feldmann, J. *Appl. Phys. Lett.* **2012**, *100*, 223903.
(41) Klimov, V. I. *J. Phys. Chem. B* **2000**, *104*, 6112.
(42) Zhu, H.; Song, N.; Rodríguez-Córdoba, W.; Lian, T. *J. Am. Chem. Soc.* **2012**, *134*, 4250.
(43) Zhu, H.; Song, N.; Lian, T. *J. Am. Chem. Soc.* **2011**, *133*, 8762.
(44) Clegg, R. M. *Curr. Opin. Chem. Biol.* **1995**, *6*, 103.
(45) Stryer, L. *Annu. Rev. Biochem.* **1978**, *47*, 819.
(46) Förster, T. *Ann. Phys. (Berlin)* **1948**, *437*, 55.
(47) Wu, K.; Rodríguez-Córdoba, W. E.; Yang, Y.; Lian, T. *Nano Lett.* **2013**, *13*, 5255.
(48) O'Connor, T.; Panov, M. S.; Mereshchenko, A.; Tarnovsky, A. N.; Lorek, R.; Perera, D.; Diederich, G.; Lambright, S.; Moroz, P.; Zamkov, M. *ACS Nano* **2012**, *6*, 8156.
(49) Song, N.; Zhu, H.; Jin, S.; Zhan, W.; Lian, T. *ACS Nano* **2010**, *5*, 613.
(50) Tvrdy, K.; Frantsuzov, P. A.; Kamat, P. V. *Proc. Natl. Acad. Sci. U.S.A.* **2011**, *108*, 29.
(51) Hässelbarth, A.; Eychmüller, A.; Weller, H. *Chem. Phys. Lett.* **1993**, *203*, 271.
(52) Mooney, J.; Krause, M. M.; Saari, J. I.; Kambhampati, P. *J. Chem. Phys.* **2013**, *138*, 204705.
(53) Mooney, J.; Krause, M. M.; Saari, J. I.; Kambhampati, P. *Phys. Rev. B* **2013**, *87*, 081201.
(54) Marcus, R.; Sutin, N. *Biochim. Biophys. Acta* **1985**, *811*, 265.
(55) Bao, N.; Shen, L.; Takata, T.; Domen, K. *Chem. Mater.* **2007**, *20*, 110.
(56) Liu, M.; Jing, D.; Zhou, Z.; Guo, L. *Nat. Commun.* **2013**, DOI: 10.1038/ncomms3278.
(57) Huang, L.; Wang, X.; Yang, J.; Liu, G.; Han, J.; Li, C. *J. Phys. Chem. C* **2013**, *117*, 11584.
(58) Yan, H.; Yang, J.; Ma, G.; Wu, G.; Zong, X.; Lei, Z.; Shi, J.; Li, C. *J. Catal.* **2009**, *266*, 165.
(59) Tachibana, Y.; Akiyama, H. Y.; Ohtsuka, Y.; Torimoto, T.; Kuwabata, S. *Chem. Lett.* **2007**, *36*, 88.
(60) Zhu, H.; Song, N.; Lian, T. *J. Am. Chem. Soc.* **2013**, *135*, 11461.
(61) Brown, K. A.; Dayal, S.; Ai, X.; Rumbles, G.; King, P. W. *J. Am. Chem. Soc.* **2010**, *132*, 9672.
(62) Zhang, J.; Wang, Y.; Jin, J.; Zhang, J.; Lin, Z.; Huang, F.; Yu, J. *ACS Appl. Mater. Interface* **2013**, *5*, 10317.